

High-throughput, temperature-controlled microchannel acoustophoresis device made with rapid prototyping

Jonathan D Adams^{1,4}, Christian L Ebbesen^{2,4}, Rune Barnkob², Allen H J Yang³, H Tom Soh³ and Henrik Bruus²

¹ Department of Physics, University of California, Santa Barbara, CA 93106, USA

² Department of Micro- and Nanotechnology, Technical University of Denmark, DTU Nanotech Building 345 East, DK-2800 Kongens Lyngby, Denmark

³ Department of Mechanical Engineering, University of California, Santa Barbara, CA 93106, USA

E-mail: tsoh@engr.ucsb.edu and Henrik.Bruus@nanotech.dtu.dk

Received 3 March 2012, in final form 8 May 2012

Published 20 June 2012

Online at stacks.iop.org/JMM/22/075017

Abstract

We report a temperature-controlled microfluidic acoustophoresis device capable of separating particles and transferring blood cells from undiluted whole human blood at a volume throughput greater than 1 L h^{-1} . The device is fabricated from glass substrates and polymer sheets in microscope-slide format using low-cost, rapid-prototyping techniques. This high-throughput acoustophoresis chip (HTAC) utilizes a temperature-stabilized, standing ultrasonic wave, which imposes differential acoustic radiation forces that can separate particles according to size, density and compressibility. The device proved capable of separating a mixture of 10- and $2\text{-}\mu\text{m}$ -diameter polystyrene beads with a sorting efficiency of 0.8 at a flow rate of 1 L h^{-1} . As a first step toward biological applications, the HTAC was also tested in processing whole human blood and proved capable of transferring blood cells from undiluted whole human blood with an efficiency of 0.95 at 1 L h^{-1} and 0.82 at 2 L h^{-1} .

(Some figures may appear in colour only in the online journal)

1. Introduction

Systems for the separation and purification of particles and cells from complex mixtures have become essential tools in many areas of biological research and medicine. Microfluidics technology offers the potential for many high-performance cell-sorting applications because it allows precise manipulation of the separation forces that govern purity, recovery and throughput [1, 2]. A number of different force fields have been successfully utilized within microchannels including inertia [3], electrokinetics [4], dielectrophoretics [5], magnetophoretics [6], as well as mechanical contact forces [7].

Recently, as reviewed in [8, 9], there has been growing interest in on-chip microchannel acoustophoresis for biological applications, which allows gentle and label-free separation based on the size, density and compressibility

of particles. Examples are acoustophoretic cell separation devices [10–12], cell trapping [13–15], plasmapheresis [16], forensic analysis [17], food analysis [18], cell sorting using surface acoustic waves [19], cell synchronization [20], cell differentiation [21] and cell compressibility studies [22]. At the same time, substantial advancements in understanding the fundamental physics of biochip acoustophoresis have been achieved through full-chip imaging of acoustic resonances [23], particle handling by surface acoustic waves [24–28], multi-resonance chips [29], advanced frequency control [30, 31], on-chip integration with magnetic separators [32], acoustics-assisted microgrippers [33], acoustic programming [34], band-pass filters [35], *in situ* force calibration [36] and automated micro-PIV systems [37].

However, regardless of the separation mechanism, volume throughput limitations represent a major Achilles heel for microfluidics-based cell sorting devices. These typically exhibit volume flow rates below 0.06 L h^{-1} ($= 1 \text{ mL min}^{-1}$)

⁴ These authors contributed equally to this work.

[19, 38, 39], and this limitation has restricted the use of microfluidics technology to low-volume applications. The availability of devices capable of high volume throughput separation would open new avenues in cell-based therapies [40], environmental monitoring [41] and food-borne pathogen detection [42]. The following three papers have reported above-the-norm sample flow rates Q of about 0.3 L h^{-1} for microchannel-based acoustophoretic particle separation or transfer devices: (i) $Q = 0.3 \text{ L h}^{-1}$ for the $(100 \times 60 \times 12) \text{ mm}^3$ plexiglass/stainless steel device containing a single $(70 \times 48 \times 3) \text{ mm}^3$ broad, shallow channel with transfer ratios of 0.85–0.95 and 0.0–0.1 for a $340\text{-}\mu\text{m}$ -diameter and $200\text{-}\mu\text{m}$ -diameter polystyrene particle suspensions, respectively, [43] (20 times larger than cells); (ii) $Q = 0.2 \text{ L h}^{-1}$ for the $(70 \times 15 \times 5) \text{ mm}^3$ quartz glass/stainless steel device containing a single $(50 \times 10 \times 0.25) \text{ mm}^3$ broad, shallow channel with transfer ratio of 0.7 for $5\text{-}\mu\text{m}$ -diameter yeast cells [12] (the transfer ratio dropped to 0.3 for $Q = 1 \text{ L h}^{-1}$); and (iii) $Q = 0.24 \text{ L h}^{-1}$ for the $(55 \times 20 \times 1.5) \text{ mm}^3$ Si/glass device containing eight $(40 \times 0.38 \times 0.16) \text{ mm}^3$ narrow, shallow channels coupled in parallel with separation coefficients of 0.7–0.9 for suspensions of blood cells (BCs) and lipid particles [44]. We note that in none of these works temperature control has been applied, which, as we shall discuss below, limits a further increase of the throughput.

As a step toward addressing the compelling need for large volume separation capability in biomedical applications, we report here the high-throughput acoustophoresis chip (HTAC). The high throughput of the HTAC is obtained by combining the single broad, shallow-channel geometry [12, 43], here of dimension $(60 \times 17 \times 0.83) \text{ mm}^3$, with thermally controlled acoustofluidics [37]. The latter ensures the stability of the temperature-dependent ultrasound resonance responsible for the functionality, when operating the HTAC at relatively high ultrasound power levels. The HTAC is fabricated using a low-cost, rapid prototyping microscope-slide format of overall size $(75 \times 25 \times 4.5) \text{ mm}^3$, convenient for biotech applications, and with externally adjustable tubing for controlling the ratio of the sample and buffer flow rates. The HTAC has successfully been tested to separate polystyrene microbeads and to transfer BCs from undiluted whole human blood. We have achieved microchannel separation and transfer results comparable to those reported in the literature, but for flow rates nearly an order of magnitude higher than the previously highest reported flow rates and about two orders of magnitudes higher than the typical flow rates reported in the field.

2. Device design

2.1. HTAC device architecture

The design of the HTAC device builds on the broad, shallow-channel geometry [12, 43] and is fabricated with a low-cost, multi-layer, rapid prototyping process. The device is designed with five functional layers (bottom slide, bottom gasket, divider, top gasket, and top slide), wherein the height of the bottom gasket is half that of the top gasket to place the divider at approximately one-third of the channel height

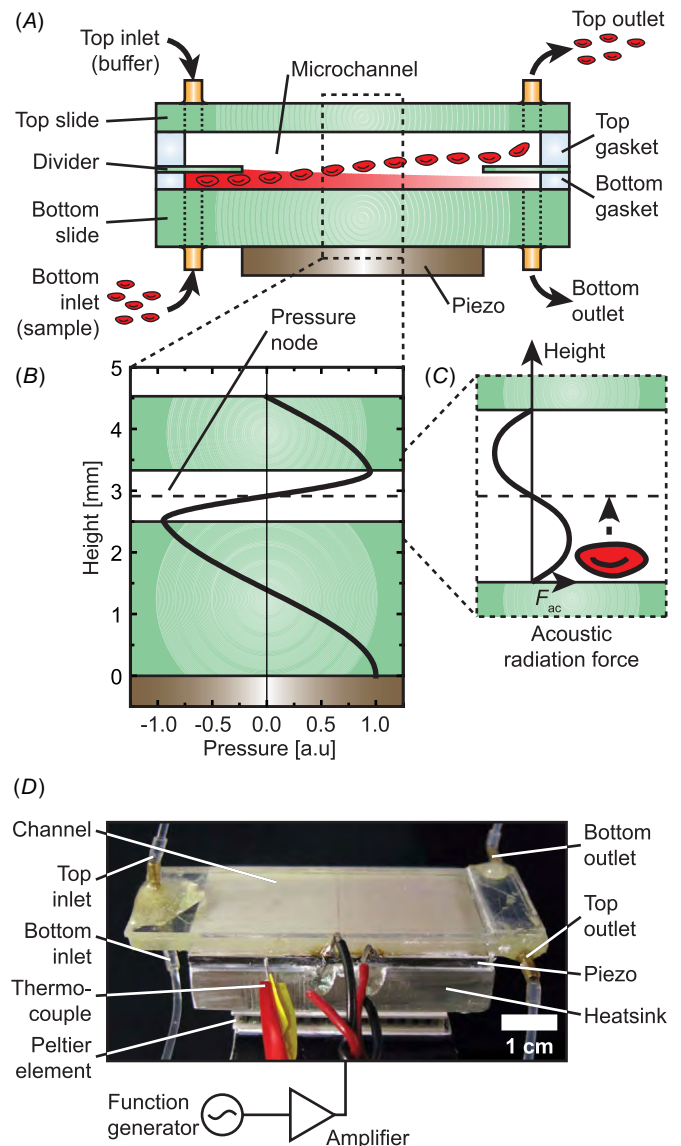


Figure 1. (A) Design schematic of the HTAC showing the microchannel formed by the bottom gasket, divider and top gasket sandwiched between the bottom and top slides. The sample suspension and buffer are injected through the bottom inlet and top inlet, respectively. (B) The device is designed to support a standing half-wave in the applied ultrasound pressure field across the height of the microchannel, with its nodal plane at half the channel height, i.e. above the flow divider at one-third the channel height. (C) The acoustophoretic force F_{ac} (sinusoidal black line) driving particles toward the nodal plane. (D) Photograph of the HTAC placed on top of the piezo transducer mounted on a Peltier element and an aluminum-block heat sink fitted with a thermocouple for thermal control.

(figure 1(A)). The details of the device fabrication and dimensions are provided in section 3.1. The sample (a polystyrene particle suspension or whole blood) and the buffer are pumped into the horizontally placed device through the bottom and top inlets, respectively, and by keeping the Reynolds number below 100, these two streams are fully laminar under the operating conditions. By adjusting the ratio of the two flow rates and relying on gravity-induced sedimentation, we ensure that no particles are transferred

between the two streams without acoustic actuation, such that the sample and buffer elute through the bottom and top outlets, respectively.

A piezo transducer is attached to the bottom slide and driven with a function generator through a custom-built amplifier to generate standing ultrasound waves of frequency f within the device. Importantly, the HTAC structure is designed such that the vertical component of the standing wave has a half-wave in the bottom slide, a half-wave in the microchannel and a quarter wave in the top slide (figure 1(B)). In this configuration, the particles experience an acoustic radiation force directed toward the horizontal nodal plane located at one-half the microchannel height—above the divider, which is situated at one-third the channel height. In this way, the strength of the acoustic field, and the magnitude of the flow rates can be adjusted to control the selective transfer of particles from the lower stream to the upper stream.

2.2. HTAC acoustic theory and design

The acoustic radiation force F_{ac} generated by the vertical standing waves of wavelength λ_o in the microchannel and acting on a particle with radius a has the sinusoidal form [45] (figure 1(C)):

$$F_{ac} = 4\pi a^3 k_o E_o \left[\frac{\rho_p + \frac{2}{3}(\rho_p - \rho_o)}{2\rho_p + \rho_o} - \frac{1}{3} \frac{\kappa_p}{\kappa_o} \right] \sin(2k_o z), \quad (1)$$

where k_o is $2\pi/\lambda_o$, z is the vertical coordinate, E_o is the energy density, ρ is density and κ is compressibility with subscripts ‘p’ and ‘o’ respectively denoting the particle and the suspension medium. Since F_{ac} depends on the particle volume, larger particles will move faster due to the radius-squared dependence on the velocity $u = F_{ac}/(6\pi\eta a)$ from balancing F_{ac} with the Stokes drag from the liquid with viscosity η . Because the particle radii in this work are larger than $1 \mu\text{m}$, the η -dependence of F_{ac} can be neglected [46].

To determine the optimal dimensions of the device components, we modeled the acoustic field in the HTAC by approximating the geometry as a parallel-plate triple layer structure (bottom slide, water-filled microchannel, top slide) placed on a piezo transducer and by considering only the dependence of the pressure field p of the vertical z coordinate. We only treat longitudinal elastic waves in the top and bottom slides, and since the viscous damping factor $\eta f \pi / (\rho_o c_o^2)$ is minute ($\approx 10^{-6}$), we neglect the viscosity of water. In this simplified 1D model, the pressure p satisfies the Helmholtz wave equation $p''(z) = -[2\pi f/c(z)]^2 p(z)$, where $c(z)$ is the speed of sound in the slides or in the liquid at position z . The boundary conditions are $p' = 0$ at the lower surface of the bottom slide facing the piezo transducer, continuity of pressure and oscillation velocity at the slide/liquid interfaces, and $p = 0$ at the top slide facing the air.

Using the material properties listed in table 1, our simulation shows that at a fixed temperature of $25 \text{ }^\circ\text{C}$ the desired optimal resonance pattern (figure 1(B)) is achieved at an operating frequency of $f = 938 \text{ kHz}$ for a pyrex bottom-slide thickness of 2.50 mm , a pyrex top-slide thickness of 1.25 mm and a channel height of 0.83 mm .

Table 1. Acoustic parameters used for modeling [47, 48].

Parameter	Symbol	T ($^\circ\text{C}$)	Value
Density, water	ρ_o	5–50	998 kg m^{-3}
Speed of sound, water	c_o	5 25 50	1424 m s^{-1} 1497 m s^{-1} 1541 m s^{-1}
Density, pyrex	ρ	5–50	2230 kg m^{-3}
Longitudinal speed of sound, pyrex	c	25	5661 m s^{-1}
Young’s modulus, pyrex	Y	5 25 50	62.4 GPa 62.6 GPa 62.8 GPa
Poisson’s ratio, pyrex	σ	5 25 50	0.2179 0.2200 0.2226

2.3. HTAC thermal theory and design

During the operation of the HTAC, the power consumption of the piezo transducer was a maximum of 10 W , which resulted in device heating. We therefore analyzed the sensitivity of the acoustic resonance to changes in temperature using numerical modeling, performing a 2D analysis in the vertical plane (neglecting effects of the finite width) of the triple layer pyrex/water/pyrex structure. All simulations were performed using Comsol Multiphysics (COSMOL, www.comsol.com), and convergence tests were performed showing that more than $500\,000$ degrees of freedom were needed to ensure a mesh-independent result. Given the approximation of the device geometry, the numerical uncertainty of the results is estimated to be 5% .

First, we calculated the temperature profile in the HTAC. We found that the sample and buffer injected at room temperature act as cooling water preventing the top slide from being heated, resulting in a roughly linear temperature change from T_{pz} , the temperature of the piezo transducer, at the bottom of the bottom slide to room temperature at the top of the microchannel. Using this temperature profile, we then calculated the thermal sensitivity of the acoustic resonances in terms of the acoustic energy density E_o in the water from a standard acoustic model [49]: the equations of motion for the elastic displacement field u of the pyrex slides coupled with the Helmholtz wave equation for the pressure p of the water in the microchannel,

$$\nabla^2 \mathbf{u} + \frac{\nabla(\nabla \cdot \mathbf{u})}{1 - 2\sigma} = -\frac{2(1 + \sigma)\rho}{Y} [(1 + i\gamma)\omega]^2 \mathbf{u}, \quad (2)$$

$$\nabla^2 p = -\frac{1}{c_o^2} [(1 + i\gamma)\omega]^2 p. \quad (3)$$

Here, c_o is the speed of sound of water, while Y , σ and ρ is Young’s modulus, Poisson’s ratio and density of the pyrex, respectively. The temperature dependence of these parameters are listed in table 1. To model the dissipation of acoustic energy due to radiation as well as friction in the bulk and in the boundary layers, we have followed [36, 50] and multiplied the angular frequency by the complex-valued damping factor $(1 + i\gamma)$ with $\gamma = 10^{-3}$. This corresponds

to experimentally obtained Q values [36] of the acoustic resonances, $Q = 1/(2\gamma) \approx 500$.

The resulting energy density $E_o(f)$ at a given temperature T_{pz} exhibited a Lorentzian resonance peak [36] with center frequency $f_o(T_{pz})$ and a full peak width at half-maximum Δf_{FW} . At $T_{pz} = 25^\circ\text{C}$, we determined a center frequency of $f_o = 938$ kHz (in agreement with our previous 1D model) and a peak width $\Delta f_{FW} = 4$ kHz. Importantly, we found that the thermal sensitivity of the resonance mode was $[f_o(T_{pz} + \Delta T) - f_o(T_{pz})]/\Delta T \sim 0.4$ kHz $^\circ\text{C}^{-1}$ corresponding to a displacement of f_o by a full peak width Δf_{FW} per 10°C . We further calculated that such a shift in f leads to a reduction in E_o by about a factor of 20. This numerical estimate, combined with equation (1) and experimental observations, led us to conclude that active temperature control is critical for maintaining device functionality; without active temperature control, heating of the device from the piezo transducer would shift the acoustic resonance thereby significantly decreasing the acoustic energy and result in poor separation efficiency. Thus, we incorporated an active Peltier cooling element with an aluminum heat sink fitted with a thermocouple, so that the interface between the piezo transducer and the bottom slide was maintained at 25°C (figure 1(D)).

3. Device fabrication, setup and experimental procedures

3.1. Device fabrication

Our device consists of a single broad and shallow microchannel ($60\text{ mm} \times 17\text{ mm} \times 0.83\text{ mm}$) equipped with two inlet/outlet pairs and fabricated from PDMS gaskets, cut from $250\text{ }\mu\text{m}$ thick PDMS sheets using a plotting cutter (Graphtec America Inc., www.graphtecamerica.com), plasma bonded between standard $25\text{ mm} \times 75\text{ mm}$ glass microscope slides of thickness 1.25 mm (Fisher Scientific, www.fishersci.com). Two bottom slides are bonded together using 5-minute-epoxy glue. Together with the single-thickness top slide, they act as acoustic reflectors. The central flow divider is milled from a $150\text{ }\mu\text{m}$ thick borofloat glass wafer (Mark Optics, www.markoptics.com) using a CNC mill (Flashcut CNC, www.flashcutcnc.com), and etched in 49% HF to a final thickness of $70\text{ }\mu\text{m}$. To avoid working with the toxic HF etchant, one could instead use a glass slide with a thickness as close as possible to $70\text{ }\mu\text{m}$ and cope with the reduced amplitude of the standing ultrasound wave resulting from the less-than-perfect height ratios. Borosilicate glass wafers only $100\text{ }\mu\text{m}$ thick are now commercially available from SCHOTT North America Inc. Alternatively, one could use a thin polymer sheet with sufficiently high stiffness to reduce the generation of acoustic streaming (leading to unwanted mixing of the flow streams) from vibrations of its edges. Two $27\text{ mm} \times 27\text{ mm}$ piezoelectric transducers (Ferropem Piezoceramics, www.ferropem-piezo.com), fully covering the separation channel, are attached on the underside of the device using superglue and induce a strong acoustic resonance in the microchannel when powered by a sinusoidal voltage at 899 kHz and an amplitude of up to 55 V (all

voltages in this paper are peak-to-peak values), using a custom-built amplifier based on bridged LT1210 op-amps (Linear Technology, www.linear.com).

3.2. Experimental setup

The device is mounted in a stable fluidic setup with $500\text{-}\mu\text{m}$ -diameter teflon tubing (Upchurch Scientific, www.idex-hs.com/Upchurch-Scientific.aspx). The hydraulic resistance (length) of the outlet tubing is matched to ensure a correct sample: buffer flow ratio of 1:2, which for the whole human blood was achieved by adjusting the length of the outer tubing with the acoustics on. Two and six parallel-coupled syringe pumps (Harvard Apparatus, www.harvardapparatus.com) inject sample and buffer solutions into the system, respectively, achieving a maximum flow rate of 2 L h^{-1} sample and 6 L h^{-1} buffer. The temperature of the bottom surface of the device is measured using a chromel/alumel thermocouple (Omega Engineering Inc., www.omega.com). The device is mounted in thermal compound on an aluminum heat sink and cooled by a Peltier element with a power consumption of typically 2 W . To reduce separation degradation from acoustic streaming near the flow divider [51], we sweep the frequency linearly in 1 ms periods from 10 kHz below to 10 kHz above the center frequency [30], corresponding to about twice the peak width Δf_{FW} .

3.3. Fluorescent polystyrene bead sample

$2\text{-}\mu\text{m}$ -diameter red fluorescent and $10\text{-}\mu\text{m}$ -diameter green fluorescent beads were purchased from Microgenics (www.microgenics.com). A degassed solution consisting of DI water with surfactant (0.01% v/v Tween-20) added to reduce nonspecific adhesion of beads was used as a buffer (unless indicated, all reagents were obtained from Sigma). Sample solutions were prepared by suspending the beads at a total concentration of 10^6 beads/mL in the buffer solution. Following separation, outlet samples that were collected in microcentrifuge tubes were directly analyzed via flow cytometry (Accuri Cytometers) to quantitate separation performance.

3.4. Whole human blood sample

Whole human blood purchased from Bioreclamation (www.bioreclamation.com) was used in the HTAC within five days of receipt. It was injected into the device alongside a buffer of degassed standard concentration phosphate buffered saline ($1 \times \text{PBS}$, Fisher Scientific). Collected outlet samples were diluted 100-fold in $1 \times \text{PBS}$ before being analyzed by flow cytometry for fractionation performance. To characterize the state of the BCs we analyzed resting platelets in the blood sample on the day of receipt and then quantified platelet activation post-HTAC processing within five days of receipt using the procedure described in the [appendix](#).

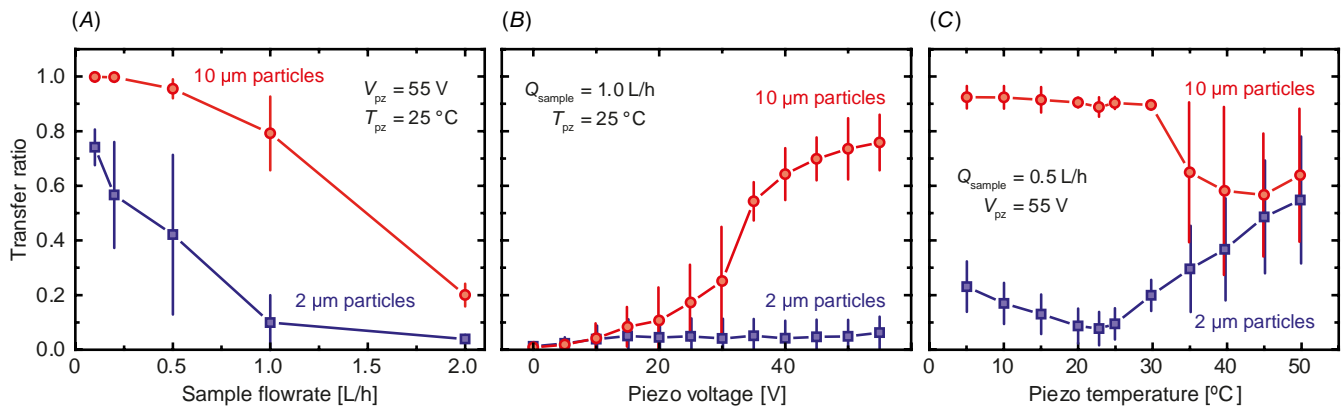


Figure 2. Transfer ratio (fraction of beads transferred from the bottom inlet to the top outlet) of 2- and 10- μm -diameter polystyrene beads at the resonance frequency of 899 kHz. Error bars are standard deviations obtained from experiments performed in triplicate. (A) Transfer ratio as a function of the sample flow rate at 25 $^{\circ}\text{C}$ and a piezo voltage of 55 V. Maximum difference in the transfer ratio was observed at 1 L h^{-1} . (B) Transfer ratio as a function of the piezo voltage at a temperature of 25 $^{\circ}\text{C}$ and the sample flow rate of 1.0 L h^{-1} . The difference in transfer ratios increases monotonically. (C) Transfer ratio as a function of piezo temperature shows optimal operation between 20 and 25 $^{\circ}\text{C}$. Above 45 $^{\circ}\text{C}$, the transfer ratio approaches 0.66 corresponding to equal particle density in both outlets (total mixing) and reflecting the 2:1 outlet flow rate ratio between the buffer and the sample.

4. Results

4.1. Bead separation performance

Using the suspension of fluorescent polystyrene beads (section 3.3), we characterized the purity and throughput of the HTAC. The sample and buffer were injected by syringe pumps into the device at a flow ratio of 1:3, and the outlet tubing lengths were adjusted to maintain a top:bottom outlet flow ratio of 1:2. The HTAC was operated at the experimentally determined resonance at $f = 899$ kHz, which was only 4% lower than the theoretically predicted $f_0 = 938$ kHz. We used this frequency throughout the experiments. Eluents from outlets were collected in microcentrifuge tubes and were measured with flow cytometry. We define the transfer ratio for a given type of particle as the number of particles in the top outlet relative to the total number of particles in both the top and bottom outlets.

We first measured the dependence of the transfer ratio on the flow rate, keeping the piezo temperature constant at 25 $^{\circ}\text{C}$ and the applied voltage constant at 55 V (figure 2(A)). At low flow rates (below 0.5 L h^{-1}) we observe that both particle types have sufficient transit time to get transferred from the lower inlet to the upper outlet (both transfer ratios are above 0.5). Conversely, at the high flow rate (2.0 L h^{-1}) the transfer ratios of both particle types were below 0.2. A successful separation (a large difference in transfer ratios) was observed at a sample flow rate of 1.0 L h^{-1} , where the transfer ratios are 0.8 and 0.1 for the 10- and 2- μm -diameter microbeads, respectively.

We note that the transfer ratio can be adjusted by the piezo voltage V_{pz} because it controls E_0 . At the sample flow rate of 1.0 L h^{-1} and at the piezo temperature of 25 $^{\circ}\text{C}$, we observe that the difference in transfer ratios increases monotonically as a function of the piezo voltage and saturates near 55 V where the transfer ratios are 0.8 and 0.1 for the 10- and 2- μm -diameter microbeads, respectively (figure 2(B)).

Finally, in figure 2(C), we demonstrate the importance of piezo temperature control by plotting the transfer ratio

as a function of temperature at a constant sample flow rate of 0.5 L h^{-1} , and at a constant piezo voltage of 55 V. We observe a maximal difference in the transfer ratio at 25 $^{\circ}\text{C}$. For some biological experiments it would be desirable to have an optimal transfer ratio at a temperature of 4 or 37 $^{\circ}\text{C}$. For such applications, the HTAC operation can be readily adjusted by tuning the temperature settings and the driving frequency.

The data in the three panels were taken on different days. All data points acquired under the same settings agree within the error bars, except the 2- μm -diameter bead at $Q_{\text{sample}} = 0.5$ L h^{-1} and $T_{\text{pz}} = 25$ $^{\circ}\text{C}$. For this point the error bars in panel (A) and (C) barely overlap.

4.2. Blood cell transfer performance

As a step toward biotech applications, we used the HTAC to transfer BCs from the whole human blood sample (section 3.4) into the buffer in a continuous flow manner (figure 3(A)). The idea was to test whether the HTAC could handle the high viscosity and high cell concentration of such a realistic sample, a difficult issue often bypassed in on-chip handling of blood by using diluted samples [9]. We also wanted to test, if suspended cells would be damaged by the large shear forces due to the high flow rate. Due to the large difference in viscosity between whole blood and 1 \times PBS buffer, we adjusted the relative lengths of the outlet tubing sections to retain a top:bottom outlet flow ratio of 1:2. As a negative control, the HTAC was operated without activating the piezo transducer. We found a transfer ratio of BCs to be negligible (figure 3(B) blue line). Next, we operated the HTAC at a piezo voltage of 55 V and a piezo temperature of 25 $^{\circ}\text{C}$, and measured the BC transfer ratio as a function of the flow rate from 0.1 to 2 L h^{-1} (figure 3(B) red line).

Remarkably, we found the transfer ratio of BCs in whole blood to be 0.95 for sample flow rates up to 1 L h^{-1} , which decreased slightly to 0.82 at 2 L h^{-1} . We note, that at this latter sample flow rate, the buffer flow rate is about 6 L h^{-1} , and our device thus carries a total flow rate of 8 L h^{-1} . Interestingly, the

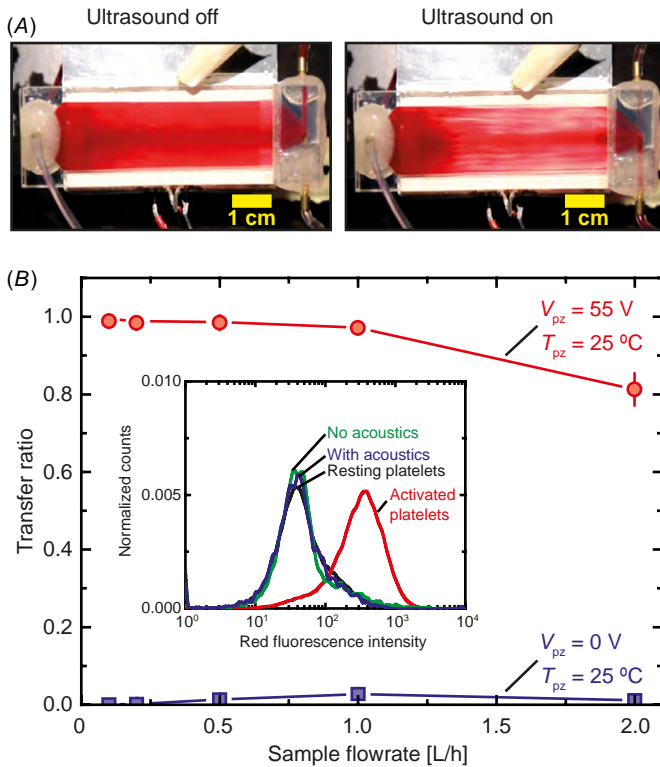


Figure 3. Separation of whole blood samples. (A) During operation at a sample flow rate of 0.5 L h^{-1} and a buffer flow rate of 1.5 L h^{-1} , whole blood is injected into the lower half of the device. From there, by the acoustic radiation force from the piezo-induced ultrasound standing wave, the BCs are lifted up into the upper half of the device, forming clearly visible red stripes due to transverse components of the standing ultrasound wave, and leave through the top outlet. (B) Measured acoustophoretic transfer of BCs from the undiluted whole blood in the bottom inlet to the buffer top outlet as a function of the flow rate at 25°C with acoustics ($V_{pz} = 55\text{V}$, top curve) and without ($V_{pz} = 0\text{V}$, bottom curve). The inset shows red fluorescence for platelets stained with red fluorescent anti-CD62-PE. Activation is not induced by passage through the device either without (green) or with (blue) the presence of the ultrasound field as compared to resting platelets (black) and pro-thrombin-activated platelets (red).

transfer ratio of BCs was higher than that of $10\text{-}\mu\text{m}$ -diameter polystyrene particles at sample flow rates above 1 L h^{-1} . We speculate that this could be due to many-particle effects, as the concentration of red BCs is approaching a magnitude beyond which a previous model study has shown that hydrodynamic many-particle interaction can cause enhanced transfer of particles [52].

To investigate whether the HTAC device damaged the cells or affected their viability, we measured the activation of platelets in whole blood as described in the appendix. To do so, the expression level of CD62 was measured with flow cytometry by labeling the platelets with CD62-PE antibody (figure 3(B) inset). The counts obtained in each bin for each curve were normalized by the total counts for that curve. Prothrombin-activated platelets show highest level of CD62 expression (isolated red curve on the right). In comparison, platelets processed without (green) and with (blue) acoustic actuation (at piezo voltage of 55 V and temperature of 25°C) show negligible differences in CD 62 expression compared to resting platelets (black). Since platelet activation is known to

be highly sensitive to mechanical forces, we extrapolate that the HTAC has minimal effect on the other blood cells.

5. Conclusion

In this work, we have described the HTAC, a temperature controlled, microfluidic acoustophoresis device capable of continuously separating microparticles and transferring BCs from undiluted whole human blood into a buffer at a volume throughput in excess of 1 L h^{-1} , one to two orders of magnitude higher than previous approaches. Importantly, we have shown that despite the high flow rate, our label-free separation method is gentle on the cells, and does not activate platelets when whole blood is processed through the device. From experiments and numerical simulations, we have discovered that active temperature control is critical for sustained device function. Without active control, the heat from the piezo transducer, driven at the high voltage necessary for achieving high throughput, causes significant shifts in the acoustic resonance frequency, rendering the device inoperative.

Central to the design of HTAC are the laminar, low aspect-ratio, co-flowing sample and buffer streams in the device kept at a fixed temperature. The cross-sectional geometry of the channel featuring a shallow height ($830 \mu\text{m}$) enables precise formation of ultrasound standing waves that vertically transport the target cells, while a large perpendicular width (17 mm) enables high-volume flow rates. Importantly, miniaturization in our device design not only ensures laminar flow but it also allows efficient generation of acoustophoretic forces by ultrasound: (i) the sub-millimeter vertical dimension of the HTAC supports a half-wavelength standing wave resonance in the channel, (ii) the acoustophoretic force scales inversely proportional with the acoustic wavelength (see equation (1)) and (iii) at ultrasound frequencies the formation of air bubbles is minimized, which is important for sustained, reproducible operation of the device.

Given the high flow rate of 1 L h^{-1} , the obtained transfer ratios of $0.8:0.1$ for the $10:2\text{-}\mu\text{m}$ -diameter bead suspension are comparable to or better than those obtained in the three previous high flow-rate studies [12, 43, 44] performed at much lower flow rates $0.2\text{--}0.3 \text{ L h}^{-1}$ as quoted in the introduction. The separation sensitivity can be improved by a serial connection of two or more HTACs or by including an acoustic pre-focusing step just after the inlet inside a single HTAC. Such a pre-focusing step increases the control of the particle motion, as it would place all incoming particles at the same vertical position in the parabolic flow profile of the channel and thus ensure they all have more equal velocities before they reach the region where the transfer to the buffer stream sets in.

The capability of the HTAC to function with the viscous, undiluted, whole blood at high sample flow rates is notable. The measured transfer ratio 0.95 of BCs from undiluted whole blood at the high sample flow rate of 1 L h^{-1} in the HTAC is on par with most blood handling microdevices running with flow rates lower than 0.06 L h^{-1} . The majority of the latter works (quoted in the introduction) were even done with diluted samples, which are easier to handle. One prominent

example of a chip handling undiluted whole blood is the plasmapheresis chip developed in 2009 by Lenshof *et al* and applied for prostate-specific antigen microarray diagnostics [16]. In that work, undiluted whole blood was injected at the low flow rate of 1 mL h^{-1} and BCs were transferred out of this sample stream by acoustophoresis leaving high-quality plasma for diagnostics. Clearly, the HTAC offers an appealing starting point for the development of a plasmapheresis chip with a 1000-fold increase in the sample flow rate.

Although it is beyond the scope of this work, we envision that the device architecture shown here can be further developed to achieve fractionation of different cell types (i.e. thrombocytes, erythrocytes and leukocytes) with higher purities, target cell recoveries at higher volume throughput. Toward this end, we believe that further insights into the effects of acoustic streaming (e.g. on sub-micron particles) as well as particle–particle interactions within high-density samples may hold the key toward higher separation performance.

Acknowledgments

This research was supported by the Danish Council for Independent Research, Technology and Production Sciences, grant no. 274-09-0342, National Institutes of Health (NIH) and ARO institute of Collaborative Biotechnologies (ICB).

Appendix. Platelet activation analysis

To prepare platelet samples for activation analysis, the whole blood (section 3.4) was centrifuged at $75 \times g$ for 20 min. For resting platelets, the platelet-rich plasma was extracted and Prostaglandin E1 (PGE_1) was added to a final concentration of $10 \mu\text{M}$. A fraction of the sample was mixed with an equal volume of 2% v/v formaldehyde and incubated for 10 min to fix the resting platelets. The other fraction of the sample was diluted ten-fold in $1 \times \text{PBS}$ and injected into the HTAC device alongside a buffer of $1 \times \text{PBS}$. For the ‘acoustics on’ sample, the device was run at a frequency as described in section 3.2 and an amplitude of 55 V. The device output was collected in microcentrifuge tubes. Samples were then fixed by mixing with an equal volume of 2% v/v formaldehyde and incubating for 10 min. To prepare activated platelets, the platelet-rich plasma was removed and washed in 30% human albumin at $75 \times g$ and resuspended in $1 \times \text{PBS}$ with 2 mM EDTA. Prothrombin (Haematologic Technologies) was added to the cell suspension at a final concentration of $5 \mu\text{M}$ and the mixture was incubated at room temperature for 10 min to activate the platelets. We then added an equal volume of 2% formaldehyde and the suspension, and incubated the mixture for 30 min at room temperature to fix the platelets. The cells were then washed twice in $1 \times \text{PBS}$ solution. We fluorescently labeled the various platelet samples by adding $20 \mu\text{L}$ of anti-CD62-PE (BD Pharmingen) per $100 \mu\text{L}$ platelet suspension, and incubated the mixtures in the dark for 30 min at room temperature. We washed the suspensions twice at $75 \times g$ and added $500 \mu\text{L}$ of the PBS solution to complete the final suspensions. All samples were then analyzed by flow cytometry for activation level.

References

- [1] Adams J D and Soh H T 2009 *J. Assoc. Lab. Autom.* **14** 331
- [2] Lenshof A and Laurell T 2010 *Chem. Soc. Rev.* **39** 1203
- [3] Mach A J and Di Carlo D 2010 *Biotechnol. Bioeng.* **107** 302
- [4] Jacobson S, Hergenroder R, Koutny L and Ramsey J 1994 *Anal. Chem.* **66** 1114
- [5] Gascoyne P R C, Noshari J, Anderson T J and Becker F F 2009 *Electrophoresis* **30** 1388
- [6] Gijs M A M 2004 *Microfluidics Nanofluidics* **1** 22
- [7] Huang L, Cox E, Austin R and Sturm J 2004 *Science* **304** 987
- [8] Friend J and Yeo L Y 2011 *Rev. Mod. Phys.* **83** 647
- [9] Bruus H, Dual J, Hawkes J, Hill M, Laurell T, Nilsson J, Radel S, Sadhal S and Wiklund M 2011 *Lab Chip* **11** 3579
- [10] Petersson F, Nilsson A, Holm C, Jönsson H and Laurell T 2004 *Analyst* **129** 938
- [11] Petersson F, Nilsson A, Holm C, Jönsson H and Laurell T 2005 *Lab Chip* **5** 20
- [12] Hawkes J J, Barber R W, Emerson D R and Coakley W T 2004 *Lab Chip* **4** 446
- [13] Hultström J, Manneberg O, Dopf K, Hertz H M, Brismar H and Wiklund M 2007 *Ultrasound Med. Biol.* **33** 145
- [14] Evander M, Johansson L, Lilliehorn T, Piskur J, Lindvall M, Johansson S, Almqvist M, Laurell T and Nilsson J 2007 *Anal. Chem.* **79** 2984
- [15] Svennebring J, Manneberg O, Skafte-Pedersen P, Bruus H and Wiklund M 2009 *Biotechnol. Bioeng.* **103** 323
- [16] Lenshof A, Ahmad-Tajudin A, Jaras K, Sward-Nilsson A M, Aberg L, Marko-Varga G, Malm J, Lilja H and Laurell T 2009 *Anal. Chem.* **81** 6030
- [17] Norris J V, Evander M, Horsman-Hall K M, Nilsson J, Laurell T and Landers J P 2009 *Anal. Chem.* **81** 6089
- [18] Grenvall C, Augustsson P, Folkenberg J R and Laurell T 2009 *Anal. Chem.* **81** 6195
- [19] Franke T, Braunmueller S, Schmid L, Wixforth A and Weitz D A 2010 *Lab Chip* **10** 789
- [20] Thevoz P, Adams J D, Shea H, Bruus H and Soh H T 2010 *Anal. Chem.* **82** 3094
- [21] Augustsson P, Barnkob R, Grenvall C, Deierborg T, Brundin P, Bruus H and Laurell T 2010 *Proc. 14th MicroTAS (Groningen, The Netherlands, 3–7 Oct. 2010)* ed S Verpoorte, H Andersson, J Emneus and N Pamme pp 1337–39 (CBMS) http://www.rsc.org/binaries/LOC/2010/PDFs/Papers/456_0474.pdf
- [22] Hartono D, Liu Y, Tan P L, Then X Y S, Yung L Y L and Lim K M 2011 *Lab Chip* **11** 4072
- [23] Hagsäter S M, Jensen T G, Bruus H and Kutter J P 2007 *Lab Chip* **7** 1336
- [24] Shi J, Mao X, Ahmed D, Colletti A and Huang T J 2008 *Lab Chip* **8** 221
- [25] Shi J, Huang H, Stratton Z, Huang Y and Huang T J 2009 *Lab Chip* **9** 3354
- [26] Tan M K, Tjeung R, Ervin H, Yeo L Y and Friend J 2009 *Appl. Phys. Lett.* **95** 134101
- [27] Tan M K, Yeo L Y and Friend J R 2010 *Appl. Phys. Lett.* **97** 234106
- [28] Shi J, Yazdi S, Lin S C S, Ding X, Chiang I K, Sharp K and Huang T J 2011 *Lab Chip* **11** 2319
- [29] Manneberg O, Hagsäter S M, Svennebring J, Hertz H M, Kutter J P, Bruus H and Wiklund M 2009 *Ultrasonics* **49** 112
- [30] Manneberg O, Vanherberghen B, Onfelt B and Wiklund M 2009 *Lab Chip* **9** 833
- [31] Glynn-Jones P, Boltryk R J, Harris N R, Cranny A W J and Hill M 2010 *Ultrasonics* **50** 68
- [32] Adams J D, Thevoz P, Bruus H and Soh H T 2009 *Appl. Phys. Lett.* **95** 254103
- [33] Oberti S, Moeller D, Neild A, Dual J, Beyeler F, Nelson B J and Gutmann S 2010 *Ultrasonics* **50** 247

- [34] Ratier C and Hoyos M 2010 *Anal. Chem.* **82** 1318
- [35] Adams J D and Soh H T 2010 *Appl. Phys. Lett.* **97** 064103
- [36] Barnkob R, Augustsson P, Laurell T and Bruus H 2010 *Lab Chip* **10** 563
- [37] Augustsson P, Barnkob R, Wereley S T, Bruus H and Laurell T 2011 *Lab Chip* **11** 4152
- [38] Nilsson J, Evander M, Hammarström B and Laurell T 2009 *Anal. Chim. Acta* **649** 141
- [39] Gossett D R, Weaver W M, Mach A J, Hur S C, Tse H T K, Lee W, Amini H and Di Carlo D 2010 *Anal. Bioanal. Chem.* **397** 3249
- [40] Mancardi G and Saccardi R 2008 *Lancet Neurol.* **7** 626
- [41] Lemarchand K, Masson L and Brousseau R 2004 *Crit. Rev. Microbiol.* **30** 145
- [42] Neethirajan S, Kobayashi I, Nakajima M, Wu D, Nandagopal S and Lin F 2011 *Lab Chip* **11** 1574
- [43] Johnson D and Feke D 1995 *Separations Technol.* **5** 251
- [44] Jönsson H, Holm C, Nilsson A, Petersson F, Johnsson P and Laurell T 2004 *Ann. Thorac. Surg.* **78** 1572
- [45] Yosioka K and Kawasima Y 1955 *Acustica* **5** 167
- [46] Settnes M and Bruus H 2012 *Phys. Rev. E* **85** 016327
- [47] CRCnetBASE Product 2012 *CRC Handbook of Chemistry and Physics* 92nd edn (London: Taylor and Francis)
- [48] Spinner S 1956 *J. Am. Ceram. Soc.* **39** 113
- [49] Dual J and Schwarz T 2012 *Lab Chip* **12** 244
- [50] Groschl M 1998 *Acustica* **84** 432
- [51] Hagsäter S M, Lenshof A, Skafte-Pedersen P, Kutter J P, Laurell T and Bruus H 2008 *Lab Chip* **8** 1178
- [52] Mikkelsen C and Bruus H 2005 *Lab Chip* **5** 1293